

Evidence for $B^- \rightarrow D_s^+ K^- \ell^- \bar{\nu}_\ell$ and search for $B^- \rightarrow D_s^{*+} K^- \ell^- \bar{\nu}_\ell$

J. Stypula,³³ M. Rozanska,³³ I. Adachi,⁹ K. Adamczyk,³³ H. Aihara,⁴⁹ D. M. Asner,³⁸ T. Aushev,¹⁵ A. M. Bakich,⁴³ V. Bhardwaj,³⁰ B. Bhuyan,¹⁰ M. Bischofberger,³⁰ A. Bondar,² G. Bonvicini,⁵⁴ A. Bozek,³³ M. Bračko,^{25, 16} T. E. Browder,⁸ M.-C. Chang,⁵ P. Chang,³² V. Chekelian,²⁶ A. Chen,³¹ P. Chen,³² B. G. Cheon,⁷ R. Chistov,¹⁵ I.-S. Cho,⁵⁶ K. Cho,¹⁹ Y. Choi,⁴² J. Dalseno,^{26, 45} M. Danilov,¹⁵ J. Dingfelder,¹ Z. Doležal,³ Z. Drásal,³ A. Drutskoy,¹⁵ S. Eidelman,² H. Farhat,⁵⁴ J. E. Fast,³⁸ V. Gaur,⁴⁴ N. Gabyshev,² R. Gillard,⁵⁴ Y. M. Goh,⁷ B. Golob,^{23, 16} J. Haba,⁹ K. Hayasaka,²⁹ H. Hayashii,³⁰ Y. Horii,²⁹ Y. Hoshi,⁴⁷ W.-S. Hou,³² Y. B. Hsiung,³² H. J. Hyun,²¹ T. Iijima,^{29, 28} K. Inami,²⁸ A. Ishikawa,⁴⁸ R. Itoh,⁹ M. Iwabuchi,⁵⁶ Y. Iwasaki,⁹ T. Julius,²⁷ J. H. Kang,⁵⁶ P. Kapusta,³³ T. Kawasaki,³⁵ H. Kichimi,⁹ C. Kiesling,²⁶ H. J. Kim,²¹ J. B. Kim,²⁰ J. H. Kim,¹⁹ K. T. Kim,²⁰ Y. J. Kim,¹⁹ K. Kinoshita,⁴ B. R. Ko,²⁰ P. Kodyš,³ S. Korpar,^{25, 16} R. T. Kouzes,³⁸ P. Krizán,^{23, 16} P. Krokovny,² T. Kuhr,¹⁸ T. Kumita,⁵¹ A. Kuzmin,² Y.-J. Kwon,⁵⁶ S.-H. Lee,²⁰ J. Li,⁴¹ Y. Li,⁵³ J. Libby,¹¹ C. Liu,⁴⁰ Y. Liu,⁴ Z. Q. Liu,¹² D. Liventsev,¹⁵ R. Louvot,²² K. Miyabayashi,³⁰ H. Miyata,³⁵ Y. Miyazaki,²⁸ R. Mizuk,¹⁵ G. B. Mohanty,⁴⁴ A. Moll,^{26, 45} N. Muramatsu,³⁹ E. Nakano,³⁷ M. Nakao,⁹ Z. Natkaniec,³³ C. Ng,⁴⁹ S. Nishida,⁹ K. Nishimura,⁸ O. Nitoh,⁵² T. Nozaki,⁹ S. Ogawa,⁴⁶ T. Ohshima,²⁸ S. Okuno,¹⁷ S. L. Olsen,^{41, 8} Y. Onuki,⁴⁹ P. Pakhlov,¹⁵ G. Pakhlova,¹⁵ C. W. Park,⁴² H. Park,²¹ H. K. Park,²¹ T. K. Pedlar,²⁴ R. Pestotnik,¹⁶ M. Petrič,¹⁶ L. E. Piilonen,⁵³ M. Ritter,²⁶ M. Röhrken,¹⁸ S. Ryu,⁴¹ H. Sahoo,⁸ Y. Sakai,⁹ S. Sandilya,⁴⁴ D. Santel,⁴ T. Sanuki,⁴⁸ Y. Sato,⁴⁸ O. Schneider,²² C. Schwanda,¹³ K. Senyo,⁵⁵ O. Seon,²⁸ M. E. Sevier,²⁷ M. Shapkin,¹⁴ C. P. Shen,²⁸ T.-A. Shibata,⁵⁰ J.-G. Shiu,³² B. Shwartz,² A. Sibidanov,⁴³ F. Simon,^{26, 45} P. Smerkol,¹⁶ Y.-S. Sohn,⁵⁶ A. Sokolov,¹⁴ E. Solovieva,¹⁵ S. Stanič,³⁶ M. Starič,¹⁶ M. Sumihama,⁶ T. Sumiyoshi,⁵¹ Y. Teramoto,³⁷ M. Uchida,⁵⁰ T. Uglov,¹⁵ Y. Unno,⁷ S. Uno,⁹ P. Urquijo,¹ Y. Usov,² P. Vanhoefer,²⁶ G. Varner,⁸ K. E. Varvell,⁴³ V. Vorobyev,² P. Wang,¹² X. L. Wang,¹² M. Watanabe,³⁵ Y. Watanabe,¹⁷ J. Wiechczynski,³³ K. M. Williams,⁵³ E. Won,²⁰ B. D. Yabsley,⁴³ H. Yamamoto,⁴⁸ Y. Yamashita,³⁴ Z. P. Zhang,⁴⁰ V. Zhilich,² V. Zhulanov,² and A. Zupanc¹⁸

(The Belle Collaboration)

¹University of Bonn, Bonn

²Budker Institute of Nuclear Physics SB RAS and Novosibirsk State University, Novosibirsk 630090

³Faculty of Mathematics and Physics, Charles University, Prague

⁴University of Cincinnati, Cincinnati, Ohio 45221

⁵Department of Physics, Fu Jen Catholic University, Taipei

⁶Gifu University, Gifu

⁷Hanyang University, Seoul

⁸University of Hawaii, Honolulu, Hawaii 96822

⁹High Energy Accelerator Research Organization (KEK), Tsukuba

¹⁰Indian Institute of Technology Guwahati, Guwahati

¹¹Indian Institute of Technology Madras, Madras

¹²Institute of High Energy Physics, Chinese Academy of Sciences, Beijing

¹³Institute of High Energy Physics, Vienna

¹⁴Institute of High Energy Physics, Protvino

¹⁵Institute for Theoretical and Experimental Physics, Moscow

¹⁶J. Stefan Institute, Ljubljana

¹⁷Kanagawa University, Yokohama

¹⁸Institut für Experimentelle Kernphysik, Karlsruher Institut für Technologie, Karlsruhe

¹⁹Korea Institute of Science and Technology Information, Daejeon

²⁰Korea University, Seoul

²¹Kyungpook National University, Taegu

²²École Polytechnique Fédérale de Lausanne (EPFL), Lausanne

²³Faculty of Mathematics and Physics, University of Ljubljana, Ljubljana

²⁴Luther College, Decorah, Iowa 52101

²⁵University of Maribor, Maribor

²⁶Max-Planck-Institut für Physik, München

²⁷University of Melbourne, School of Physics, Victoria 3010

²⁸Graduate School of Science, Nagoya University, Nagoya

²⁹Kobayashi-Maskawa Institute, Nagoya University, Nagoya

³⁰Nara Women's University, Nara

- ³¹*National Central University, Chung-li*
³²*Department of Physics, National Taiwan University, Taipei*
³³*H. Niewodniczanski Institute of Nuclear Physics, Krakow*
³⁴*Nippon Dental University, Niigata*
³⁵*Niigata University, Niigata*
³⁶*University of Nova Gorica, Nova Gorica*
³⁷*Osaka City University, Osaka*
³⁸*Pacific Northwest National Laboratory, Richland, Washington 99352*
³⁹*Research Center for Electron Photon Science, Tohoku University, Sendai*
⁴⁰*University of Science and Technology of China, Hefei*
⁴¹*Seoul National University, Seoul*
⁴²*Sungkyunkwan University, Suwon*
⁴³*School of Physics, University of Sydney, NSW 2006*
⁴⁴*Tata Institute of Fundamental Research, Mumbai*
⁴⁵*Excellence Cluster Universe, Technische Universität München, Garching*
⁴⁶*Toho University, Funabashi*
⁴⁷*Tohoku Gakuin University, Tagajo*
⁴⁸*Tohoku University, Sendai*
⁴⁹*Department of Physics, University of Tokyo, Tokyo*
⁵⁰*Tokyo Institute of Technology, Tokyo*
⁵¹*Tokyo Metropolitan University, Tokyo*
⁵²*Tokyo University of Agriculture and Technology, Tokyo*
⁵³*CNP, Virginia Polytechnic Institute and State University, Blacksburg, Virginia 24061*
⁵⁴*Wayne State University, Detroit, Michigan 48202*
⁵⁵*Yamagata University, Yamagata*
⁵⁶*Yonsei University, Seoul*

We report measurements of the decays $B^- \rightarrow D_s^{(*)+} K^- \ell^- \bar{\nu}_\ell$ in a data sample containing 657×10^6 $B\bar{B}$ pairs collected with the Belle detector at the KEKB asymmetric-energy e^+e^- collider. We observe a signal with a significance of 6σ for the combined D_s and D_s^* modes and find the first evidence of the $B^- \rightarrow D_s^+ K^- \ell^- \bar{\nu}_\ell$ decay with a significance of 3.4σ . We measure the following branching fractions: $\mathcal{B}(B^- \rightarrow D_s^+ K^- \ell^- \bar{\nu}_\ell) = (0.30 \pm 0.09(\text{stat})_{-0.08}^{+0.11}(\text{syst})) \times 10^{-3}$ and $\mathcal{B}(B^- \rightarrow D_s^{(*)+} K^- \ell^- \bar{\nu}_\ell) = (0.59 \pm 0.12(\text{stat}) \pm 0.15(\text{syst})) \times 10^{-3}$ and set an upper limit $\mathcal{B}(B^- \rightarrow D_s^{*+} K^- \ell^- \bar{\nu}_\ell) < 0.56 \times 10^{-3}$ at the 90% confidence level. We also present the first measurement of the $D_s^+ K^-$ invariant mass distribution in these decays, which is dominated by a prominent peak around 2.6 GeV/ c^2 .

PACS numbers: 13.20.He, 14.40.Nd

Semileptonic B decays play a key role in testing the Standard Model (SM) and in the understanding of heavy quark dynamics. In particular, they are used to determine the weak mixing parameters $|V_{qb}|$ ($q = c, u$), complementing the measurements of CP asymmetries used to verify the Cabibbo-Kobayashi-Maskawa (CKM) mechanism of the SM [1]. The tension at the level of 2 standard deviations (σ) between the values of $|V_{qb}|$ extracted from inclusive and exclusive B decays [2], as well as some discrepancies between measurements and theoretical expectations for semileptonic B decays to excited charmed mesons, may indicate problems in the theoretical tools or in the interpretation of the experimental results.

Semileptonic B decays to final states containing a $D_s^{(*)+} \bar{K}$ system [3] provide information about the poorly known region of hadronic masses above 2.46 GeV/ c^2 , covering radially excited D meson states [4]. Further exploration of this region may help solving some puzzles in semileptonic B decays [5]. Recently, BaBar reported an observation of $B^- \rightarrow D_s^{(*)+} K^- \ell^- \bar{\nu}_\ell$ (which did not distinguish between the D_s and D_s^* final states)

with a branching fraction of $\mathcal{B}(B^- \rightarrow D_s^{(*)+} K^- \ell^- \bar{\nu}_\ell) = (6.13_{-1.03}^{+1.04}(\text{stat}) \pm 0.43(\text{syst}) \pm 0.51(\mathcal{B}(D_s))) \times 10^{-4}$ [6].

In this paper, we present measurements of $B^- \rightarrow D_s^+ K^- \ell^- \bar{\nu}_\ell$ and $B^- \rightarrow D_s^{*+} K^- \ell^- \bar{\nu}_\ell$ decays using a data sample containing 657×10^6 $B\bar{B}$ pairs that were collected with the Belle detector at the KEKB asymmetric-energy e^+e^- collider [7] operating at the $\Upsilon(4S)$ resonance (center-of-mass energy $\sqrt{s} = 10.58$ GeV). The Belle detector is a large-solid-angle magnetic spectrometer consisting of a silicon vertex detector, a 50-layer central drift chamber, a system of aerogel Cherenkov counters, time-of-flight scintillation counters and an electromagnetic calorimeter comprised of CsI(Tl) crystals located inside a superconducting solenoid coil that provides a 1.5 T magnetic field. An iron flux return located outside the coil is instrumented to identify K_L^0 mesons and muons. A detailed description of the detector can be found in Ref. [8]. We use Monte Carlo (MC) simulations to estimate signal efficiencies and background contributions. Large signal samples of $B^- \rightarrow D_s^{(*)+} K^- \ell^- \bar{\nu}_\ell$ decays are generated with the EvtGen package [9], using

a phase space model and the ISGW2 model [10] including the resonances that can decay to $D_s^{(*)}\bar{K}$. Radiative effects are modeled by PHOTOS [11]. MC samples equivalent to about ten (six) times the accumulated data are used to evaluate the background from $B\bar{B}$ (continuum $q\bar{q}$, where $q = u, d, s, c$) events.

In the analysis, we use charged tracks with impact parameters that are consistent with an origin at the beam spot and have transverse momenta above 50 MeV/c. Masses are assigned using information from particle identification subsystems. The efficiency for kaon (pion) identification ranges from 84% to 98% (92% to 94%) depending on the track momentum with a pion (kaon) misidentification probability of about 8% (16%). Electrons and muons are selected with an efficiency of about 90% and a misidentification rate below 0.2% (e) and 1.4% (μ). The momenta of particles identified as electrons are corrected for bremsstrahlung by adding photons within a 50 mrad cone around the charged particle's trajectory.

D_s^+ candidates are reconstructed in the cleanest decay chain: $D_s^+ \rightarrow \phi\pi^+$, $\phi \rightarrow K^+K^-$ ($2.32 \pm 0.14\%$ product branching fraction) and subjected to a vertex fit. We accept candidates in the invariant mass range of $1.934 \text{ GeV}/c^2 < M_{D_s} < 2.003 \text{ GeV}/c^2$, and define the signal window within $\pm 14 \text{ MeV}/c^2$ around the world average D_s mass [12]. The width of this window corresponds to 4σ of the reconstructed D_s mass, using the resolution determined from control samples in data (mentioned later). The regions outside the signal window are considered as M_{D_s} sidebands. D_s^+ candidates are combined with photons with an energy $E_\gamma > 125 \text{ MeV}$ to form D_s^{*+} candidates, subjected to a mass constrained vertex fit. Throughout this paper, all kinematic variables are defined in the $\Upsilon(4S)$ rest frame, unless otherwise stated. D_s^{*+} candidates with an invariant mass in the range of $2.079 \text{ GeV}/c^2 < M_{D_s^*} < 2.155 \text{ GeV}/c^2$ are accepted for further analysis. The signal window is defined as $2.087 \text{ GeV}/c^2 < M_{D_s^*} < 2.137 \text{ GeV}/c^2$ (3.7σ in $M_{D_s^*}$). Signal candidates for the decays considered here (B_{sig}) are formed by combining a negatively charged kaon and lepton (e or μ) with a $D_s^{(*)+}$ candidate. In the case of multiple B_{sig} candidates (22% of events after final selection requirements have multiple B_{sig} candidates), the one with the greatest confidence level of the vertex fit is chosen. Events with accepted $D_s^{*+}K^-\ell^-$ candidates (D_s^* sample) are removed from the set of $D_s^+K^-\ell^-$ candidates (D_s sample). Another charge configuration, $D_s^{(*)+}K^+\ell^-$, populated by decays of the type $B \rightarrow D_s^{(*)+}\bar{D}^{(*)}$, $\bar{D} \rightarrow \ell^-\bar{\nu}_\ell K^+X$, is used as a control sample.

Signal events are identified using the variable X_{mis} , introduced in Ref. [13] and defined as: $X_{\text{mis}} \equiv (E_{\text{beam}} - E_{D_s K \ell} - |\vec{p}_{D_s K \ell}|)/\sqrt{E_{\text{beam}}^2 - m_{B^+}^2}$, where E_{beam} is the beam energy, $E_{D_s K \ell}$ and $\vec{p}_{D_s K \ell}$ denote the total energy and momentum of the $D_s K \ell$ system, respectively, and

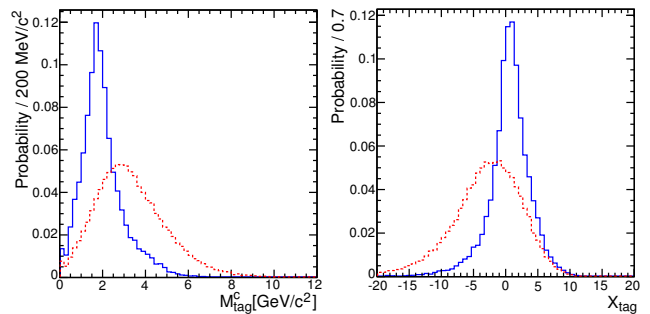


FIG. 1: M_{tag}^c (left) and X_{tag} (right) distributions for signal (blue, solid) and background (red, dashed) MC.

m_{B^+} is the nominal B^+ mass. For decays with at most one massless invisible particle, as expected for the signal, X_{mis} takes values in the range of $[-1, 1]$, defined as the signal region, while the background has a much broader distribution. X_{mis} is calculated with the four-momentum of the D_s both in the D_s and D_s^* samples, causing a small shift of X_{mis} toward higher values for the D_s^* case due to the additional low-energy photon. With this definition, the X_{mis} distribution is more robust against imperfect modeling of photon spectra in MC and simplifies the signal extraction.

Particles not assigned to the B_{sig} are used to reconstruct the tagging side of the event (B_{tag}). Exploiting the information given by B_{tag} allows for background suppression without assumptions on the (unknown) signal dynamics. We require zero total event charge as well as a negatively charged lepton with a momentum above 0.5 GeV/c on the tagging side. This reduces the main background, where a D_s^+ produced in a decay of the type $B \rightarrow D_s^{(*)+}\bar{D}^{(*)}$ is combined with a lepton and a kaon from the subsequent D decay in a semileptonic decay $\bar{B} \rightarrow \ell^-\bar{\nu}_\ell D^{(*)}X$ of the accompanying \bar{B} meson. Further improvement of the sensitivity is achieved with two tagging side variables $M_{\text{tag}}^c \equiv \sqrt{(E_{\text{tag}} - E_{\text{tag}}^\ell)^2 - (\vec{p}_{\text{tag}} - \vec{p}_{\text{tag}}^\ell)^2}$ and $X_{\text{tag}} \equiv (E_{\text{beam}} - E_{\text{tag}} - |\vec{p}_{\text{tag}}|)/\sqrt{E_{\text{beam}}^2 - m_{B^+}^2}$, where E_{tag} and \vec{p}_{tag} denote the total energy and momentum of all reconstructed particles not assigned to B_{sig} , and E_{tag}^ℓ and $\vec{p}_{\text{tag}}^\ell$ represent the energy and momentum of the prompt tagging lepton. Here M_{tag}^c represents the inclusively reconstructed mass of the hadronic system produced in the B_{tag} decay and X_{tag} is the tagging side equivalent of X_{mis} . The M_{tag}^c and X_{tag} distributions for signal and background are shown in Fig. 1.

In this blind analysis, the selection criteria for X_{tag} and M_{tag}^c are optimized for the D_s mode by maximizing the expected statistical significance, $N_S/\sqrt{N_S + N_B}$, where N_S (N_B) is the predicted number of signal (background) events in the $(X_{\text{mis}}, M_{D_s})$ signal window. This optimization is carried out for signal branching fractions $\mathcal{B}(B^- \rightarrow D_s^+ K^- \ell^- \bar{\nu}_\ell)$ in the range of $(0.25 - 0.50) \times 10^{-3}$

and yields similar optimal selection criteria for the whole range, namely $-2 < X_{\text{tag}} < 3$ and $M_{\text{tag}}^c < 2.4 \text{ GeV}/c^2$. N_B is evaluated considering two background categories in the D_s sample: “true D_s ” background with correctly reconstructed D_s^+ , described by the MC scaled to the integrated luminosity in data, and a “fake D_s ” component, where random track combinations are misreconstructed as D_s^+ , which is evaluated from the M_{D_s} sidebands. In the D_s^* sample, the background with true D_s is split into two parts: “true D_s^* ” with properly reconstructed D_s^{*+} and “fake D_s^* ”, where a true D_s^+ is combined with a random photon candidate. The background model is tested using distributions in the sideband regions $X_{\text{mis}} < -1$ and $X_{\text{mis}} > 1$.

The X_{mis} and $M_{D_s^{(*)}}$ distributions in data are shown in Fig. 2. Figure 3 shows the invariant mass distribution of the $D_s^+ K^-$ system, $M_{D_s K}$, for the combined D_s and D_s^* samples in the signal window and in the X_{mis} sidebands. Superimposed histograms represent the expected backgrounds. While the background model describes the experimental $M_{D_s K}$ distribution well in the X_{mis} sidebands, a clear excess over the expected background is seen in the signal region. The $M_{D_s K}$ distribution in the signal window is dominated by a prominent peak at $\approx 2.6 \text{ GeV}/c^2$, similarly to that observed in $B^- \rightarrow D_s^+ K^- \pi^-$ decays [14].

The signal yields are extracted from a simultaneous, extended unbinned maximum likelihood fit to the D_s and D_s^* samples, consisting of 2175 and 396 events, respectively. The D_s and D_s^* samples are fitted in two (X_{mis}, M_{D_s}) and three ($X_{\text{mis}}, M_{D_s}, M_{D_s^*}$) dimensions, respectively. The likelihood function is constructed as follows:

$$\mathcal{L} = e^{-(\sum_k N_k + \sum_{k'} N_{k'})} \prod_{i=1}^N [\sum_k N_k \mathcal{P}_k(x_i, y_i)] \times \prod_{i'=1}^{N^*} [\sum_{k'} N_{k'}^* \mathcal{P}_{k'}^*(x_{i'}, y_{i'}, z_{i'})],$$

where x_l, y_l, z_l denote X_{mis}, M_{D_s} and $M_{D_s^*}$ in the l^{th} event, and $N^{(*)}$ denotes the total number of events in the $D_s^{(*)}$ data sample. The index k (k') runs over the signal and background components in the D_s (D_s^*) sample; $N_k^{(*)}$ and $\mathcal{P}_k^{(*)}$ denote the number of events and the probability density functions (PDF) for each component, respectively. In the D_s sample, we consider two signal components coming from the decay $B^- \rightarrow D_s^+ K^- \ell^- \bar{\nu}_\ell$ and from the decay $B^- \rightarrow D_s^{*+} K^- \ell^- \bar{\nu}_\ell$ if a photon from the D_s^{*+} has been missed. In the D_s^* sample, we distinguish three signal components: one coming from the $B^- \rightarrow D_s^+ K^- \ell^- \bar{\nu}_\ell$ mode, where the D_s meson is associated with a random photon, and two from the $B^- \rightarrow D_s^{*+} K^- \ell^- \bar{\nu}_\ell$ mode, with true and fake D_s^* defined similarly to the background case discussed above. The coefficients $N_k^{(*)}$ for the signal components are expressed as the products $N_k^{(*)} = N_{D_s^{(*)}} f_k^{(*)}$, where $N_{D_s^{(*)}}$ denotes the total number of signal events in the $B^- \rightarrow D_s^{(*)+} K^- \ell^- \bar{\nu}_\ell$

TABLE I: The coefficients $f_k^{(*)}$, representing the signal fraction reconstructed in each component, evaluated from the signal MC.

Signal component k	Sample	$f_k^{(*)}$
$B^- \rightarrow D_s^+ K^- \ell^- \bar{\nu}_\ell$	D_s	$(84 \pm 1)\%$
	D_s^*	$(16 \pm 1)\%$
$B^- \rightarrow D_s^{*+} K^- \ell^- \bar{\nu}_\ell$	D_s^* with true D_s^*	$(21 \pm 1)\%$
	D_s^* with fake D_s^*	$(13 \pm 1)\%$
	D_s	$(66 \pm 1)\%$

modes. The coefficients $f_k^{(*)}$ (listed in Table I) represent the signal fraction reconstructed in each component and are evaluated from the signal MC. The coefficients $N_k^{(*)}$ for background components with fake D_s are evaluated from the M_{D_s} sidebands in data and are fixed in the fit. The two- (three-) dimensional PDF is parameterized as the product of two (three) one-dimensional PDFs for each variable. The validity of this parameterization has been checked with MC by examining the correlation between X_{mis} and M_{D_s} , which has been found negligible. The components with true $D_s^{(*)}$ are parameterized as a sum of two Gaussian functions in M_{D_s} or as a single Gaussian function in $M_{D_s^*}$, with means set to the world average $D_s^{(*)}$ mass values [12] and with the remaining parameters fixed from fits to control samples in data. The components with fake $D_s^{(*)}$ are parameterized as linear functions in $M_{D_s^{(*)}}$. The X_{mis} distribution of the signal components is modeled with two line shapes, one describing the two components of the $B^- \rightarrow D_s^+ K^- \ell^- \bar{\nu}_\ell$ mode and the other one describing the three components of the $B^- \rightarrow D_s^{*+} K^- \ell^- \bar{\nu}_\ell$ decay. They are parameterized using the function $C e^{-|X_{\text{mis}} - \mu|/\sigma|^n} e^{-\alpha(X_{\text{mis}} - \mu)}$, where C is a normalization coefficient and the parameters μ, σ, α and the integer parameter n are fixed from fits to the signal MC samples. The X_{mis} distributions of the background components are parameterized as bifurcated Gaussian functions with parameters fixed from the simulated $B\bar{B}$ events with generic B decays (true D_s) or from the M_{D_s} sidebands in data (fake D_s). The free parameters in the fit are the two signal yields $N_{D_s^{(*)}}$, the three background yields $N_m^{(*)}$ of the components with true D_s , and the coefficients of polynomials that describe the distributions in $M_{D_s^{(*)}}$ for the fake D_s components. The range of the fit is as shown in Fig. 2. The signal yields extracted from the fit are 84 ± 24 events for the decay $B^- \rightarrow D_s^+ K^- \ell^- \bar{\nu}_\ell$ and 41 ± 22 events for the decay $B^- \rightarrow D_s^{*+} K^- \ell^- \bar{\nu}_\ell$ with statistical significances of 3.9σ and 1.9σ , respectively. The significance is defined as $\Sigma = \sqrt{-2\ln(\mathcal{L}_0/\mathcal{L}_{\text{max}})}$, where \mathcal{L}_{max} and \mathcal{L}_0 denote the maximum likelihood value and the likelihood value for the zero signal hypothesis, respectively. The fit results are summarized in Table II and the fit projections in X_{mis} and M_{D_s} are shown in Fig. 2. The fitted signal yields are used to compute the branching

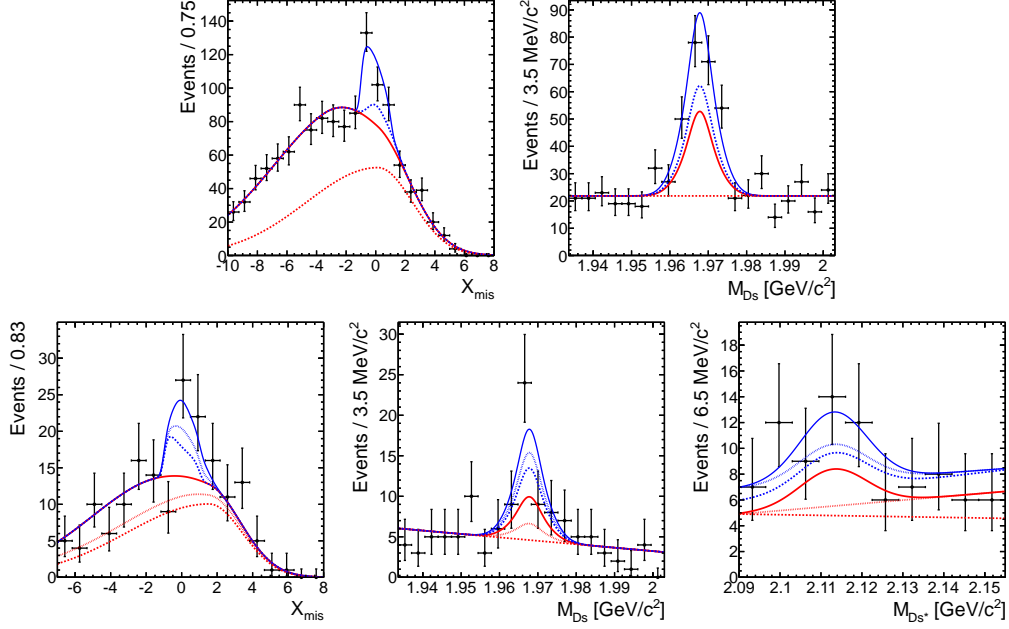


FIG. 2: Distributions (from left to right) in X_{mis} and M_{D_s} in the D_s sample (top), and X_{mis} , M_{D_s} and $M_{D_s^*}$ in the D_s^* sample (bottom). Points with error bars are the data, and lines show the fit projections. Each variable is shown in the signal region of the other variable(s). For the D_s sample the lines represent (from bottom to top) the fitted background components with fake (red dashed) and true D_s (red solid), and the signal contributions from the D_s^* (blue dashed) and D_s (blue solid) modes. For the D_s^* sample the lines (from bottom to top) represent the fitted background components with fake D_s (red dashed), fake D_s^* (red dotted), true D_s^* (red solid), and the signal contributions from the D_s mode (blue dashed), the D_s^* mode with fake D_s (blue dotted), and with true D_s^* (blue solid). The fitted contributions are superimposed additively.

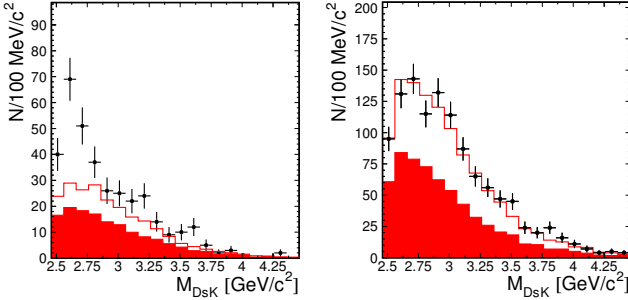


FIG. 3: The invariant mass distribution of $D_s^+ K^-$ for the combined D_s and D_s^* samples in the signal window (left) and in the X_{mis} sidebands (right). The full (blank) histograms show the expected background contribution from fake (true) D_s . The histograms are superimposed additively.

TABLE II: Signal yields ($N_{D_s^{(*)}}$), reconstruction efficiencies ($\epsilon^{(*)}$), statistical significances (Σ) and branching fractions (\mathcal{B}). The errors on the signal yields are statistical, while for the branching fractions both statistical (first) and systematic (second) errors are provided. The correlation coefficient between N_{D_s} and $N_{D_s^*}$ equals -66% .

Mode	$N_{D_s^{(*)}}$	$\epsilon^{(*)}[\%]$	Σ	$\mathcal{B} \times 10^{-3}$
$B^- \rightarrow D_s^+ K^- \ell^- \bar{\nu}_\ell$	84 ± 24	1.78	3.9	$0.30 \pm 0.09^{+0.11}_{-0.08}$
$B^- \rightarrow D_s^{*+} K^- \ell^- \bar{\nu}_\ell$	41 ± 22	0.85	1.9	$0.29 \pm 0.16^{+0.11}_{-0.10}$

fractions with the formula: $\mathcal{B}(B^- \rightarrow D_s^{(*)+} K^- \ell^- \bar{\nu}_\ell) = N_s^{(*)} / (2N_{B+B^-} \epsilon^{(*)} \mathcal{B}_{\text{int}})$, where N_{B+B^-} is the number of $B^+ B^-$ pairs in data, $\epsilon^{(*)}$ denotes the reconstruction efficiency of the signal decay chain and \mathcal{B}_{int} is the product of intermediate branching fractions set to their world average values [12]. The reconstruction efficiency is expressed as $\epsilon^{(*)} = \epsilon_{PS}^{(*)} \Delta \epsilon_{\text{cor}}^{(*)}$, where $\epsilon_{PS}^{(*)}$ is the efficiency calculated from the signal MC with the phase space model and $\Delta \epsilon_{\text{cor}}^{(*)} = 1.20$ (0.57) corrects for the difference between the data and the phase space distribution. It is calculated as a function of the effective masses of the two-body subsystems $D_s^+ K^-$, $D_s^+ \ell^-$, and $K^- \ell^-$ and averaged using the experimentally observed distributions. We obtain $\mathcal{B}(B^- \rightarrow D_s^+ K^- \ell^- \bar{\nu}_\ell) = (0.30 \pm 0.09) \times 10^{-3}$ and $\mathcal{B}(B^- \rightarrow D_s^{*+} K^- \ell^- \bar{\nu}_\ell) = (0.29 \pm 0.16) \times 10^{-3}$.

The dominant systematic uncertainty on the signal yield is due to the parameterization of the X_{mis} dependence of the signal and found to be $^{+23}_{-6}$ ($^{+7}_{-9}$) events for the D_s (D_s^*) mode. It is evaluated by refitting the data with the parameters μ , σ , and α allowed to float, and by changing the integer parameter n by ± 1 . Uncertainties in modeling the X_{mis} distributions of the background components containing true D_s are evaluated to be $^{+5}_{-7}$ ($^{+8}_{-7}$) events from fits with the background shape parameters varied by $\pm 1\sigma$, taking into account correlations between the parameters. We also repeat the fits with the param-

eters, whose values are determined from data (and which are fixed in the nominal fit), floating. The resulting uncertainty is $^{+4}_{-2}$ ($^{+0}_{-1}$) events. The effect of an imperfect estimation of the relative contributions of the signal components is determined to be ± 1 (± 1) from fits with the parameters $f_k^{(*)}$ varied by $\pm 1\sigma$ and taking into account a $\pm 3\%$ uncertainty on the photon reconstruction efficiency. The above uncertainties are summed in quadrature to obtain the total systematic uncertainty of the signal yield of $^{+24}_{-10}$ ($^{+12}_{-11}$) events for the D_s (D_s^*) modes. We include the effect of these uncertainties on the significance of the observed signals by convolving the likelihood function obtained in the fit with a Gaussian systematic error distribution. The significance of the signal in the $B^- \rightarrow D_s^+ K^- \ell^- \bar{\nu}_\ell$ ($B^- \rightarrow D_s^{*+} K^- \ell^- \bar{\nu}_\ell$) mode, after including systematic uncertainties, is 3.4σ (1.8σ).

In a similar way, we obtain a significance of 6σ for the combined $B^- \rightarrow D_s^{(*)+} K^- \ell^- \bar{\nu}_\ell$ modes from the 2-dimensional (X_{mis}, M_{D_s}) fit for the combined D_s and D_s^* samples. The much higher significance for the combined modes compared to the individual modes is due to the large cross-feed between the D_s and the D_s^* modes.

The uncertainty on the branching fractions, except for the systematic uncertainty of the signal yield, is evaluated to be 23.2% for each signal mode. It includes uncertainties in charged track reconstruction efficiency (6.6%), particle identification efficiency (3.9%), intermediate branching fractions (6.1%), number of $B^+ B^-$ pairs (1.5%) and the reconstruction efficiency correction $\Delta\epsilon_{\text{cor}}$ (21%).

The largest uncertainty, due to $\Delta\epsilon_{\text{cor}}$, is determined by calculating $\Delta\epsilon_{\text{cor}}$ in 10000 toy MC experiments. The width of a Gaussian function fitted to the obtained efficiencies is taken as systematic uncertainty. The uncertainties due to the intermediate branching fractions are taken from the errors quoted in [12]. Combining all uncertainties, we obtain $\mathcal{B}(B^- \rightarrow D_s^+ K^- \ell^- \bar{\nu}_\ell) = (0.30 \pm 0.09(\text{stat})_{-0.08}^{+0.11}(\text{syst})) \times 10^{-3}$, $\mathcal{B}(B^- \rightarrow D_s^{*+} K^- \ell^- \bar{\nu}_\ell) = (0.29 \pm 0.16(\text{stat})_{-0.10}^{+0.11}(\text{syst})) \times 10^{-3}$ and $\mathcal{B}(B^- \rightarrow D_s^{(*)+} K^- \ell^- \bar{\nu}_\ell) = (0.59 \pm 0.12(\text{stat}) \pm 0.15(\text{syst})) \times 10^{-3}$ for the combined modes obtained in a similar way, taking correlations into account. Since the significance in the D_s^* mode does not exceed 3σ , we set an upper limit of $\mathcal{B}(B^- \rightarrow D_s^{*+} K^- \ell^- \bar{\nu}_\ell) < 0.56 \times 10^{-3}$ at the 90% confidence level, using the likelihood integration method.

In conclusion, we find evidence for the decay $B^- \rightarrow D_s^+ K^- \ell^- \bar{\nu}_\ell$ with a significance of 3.4σ and measure $\mathcal{B}(B^- \rightarrow D_s^+ K^- \ell^- \bar{\nu}_\ell) = (0.30 \pm 0.09(\text{stat})_{-0.08}^{+0.11}(\text{syst})) \times 10^{-3}$. The combined $B^- \rightarrow D_s^{(*)+} K^- \ell^- \bar{\nu}_\ell$ decay modes

are observed with a significance of 6σ to be $\mathcal{B}(B^- \rightarrow D_s^{(*)+} K^- \ell^- \bar{\nu}_\ell) = (0.59 \pm 0.12(\text{stat}) \pm 0.15(\text{syst})) \times 10^{-3}$. The branching fraction results are consistent with the measurement of BaBar [6]. We also present the first measurement of the $D_s^+ K^-$ invariant mass distribution, which is dominated by a prominent peak around 2.6 GeV/ c^2 , possibly from excited D mesons decays.

We thank the KEKB group for excellent operation of the accelerator; the KEK cryogenics group for efficient solenoid operations; and the KEK computer group, the NII, and PNNL/EMSL for valuable computing and SINET4 network support. We acknowledge support from MEXT, JSPS and Nagoya's TLPSC (Japan); ARC and DIISR (Australia); NSFC (China); MSMT (Czechia); DST (India); INFN (Italy); MEST, NRF, GSDC of KISTI, and WCU (Korea); MNiSW and NCN (Poland); MES and RFAAE (Russia); ARRS (Slovenia); SNSF (Switzerland); NSC and MOE (Taiwan); and DOE and NSF (USA).

-
- [1] N. Cabibbo, Phys. Rev. Lett. **10**, 531 (1963); M. Kobayashi and T. Maskawa, Prog. Theor. Phys. **49**, 652 (1973).
 - [2] D. Asner *et al.* (Heavy Flavor Averaging Group), arXiv:1010.1589v3 [hep-ex].
 - [3] Throughout this paper, the inclusion of the charge-conjugate decay mode is implied.
 - [4] P. del Amo Sanchez *et al.* (BaBar Collaboration), Phys. Rev. D **82**, 111101(R) (2010).
 - [5] F. U. Bernlochner, Z. Ligeti, S. Turczyk, arXiv:1202.1834 [hep-ph].
 - [6] P. del Amo Sanchez *et al.* (BaBar Collaboration), Phys. Rev. Lett. **107**, 041804 (2011).
 - [7] S. Kurokawa and E. Kikutani, Nucl. Instr. and Meth. A **499**, 1 (2003), and other papers included in this volume.
 - [8] A. Abashian *et al.* (Belle Collaboration), Nucl. Instr. and Meth. A **479**, 117 (2002).
 - [9] D. J. Lange, Nucl. Instr. and Meth. A **462**, 152 (2001).
 - [10] D. Scora and N. Isgur, Phys. Rev. D **52**, 2783 (1995).
 - [11] E. Barberio and Z. Was, Comput. Phys. Commun. **79**, 291 (1994).
 - [12] K. Nakamura *et al.* (Particle Data Group), J. Phys. G **37**, 075021 (2010) and 2011 partial update for the 2012 edition.
 - [13] A. Matyja *et al.* (Belle Collaboration), Phys. Rev. Lett. **99**, 191807 (2007).
 - [14] B. Aubert *et al.* (BaBar Collaboration), Phys. Rev. Lett. **100**, 171803 (2008); J. Wiechczynski *et al.* (Belle Collaboration), Phys. Rev. D **80**, 052005 (2009).